

# Approximate boundary layer analysis and mantle convection

Physics of the Earth as a Planet, Lecture 9

## Scaling analysis of cellular convection

There is an extensive literature concerned with boundary layer analysis of convective systems, which is in general both difficult and complicated. However an idea of how the velocity and boundary layer thickness will vary with Rayleigh number can be obtained from what is essentially a scaling argument. Convection at large Rayleigh numbers driven by heating from below contains thin thermal boundary layers surrounding an isothermal core of fluid in which the vorticity is approximately constant. The vorticity decreases from the constant interior value to zero across the thickness of the boundary layers.

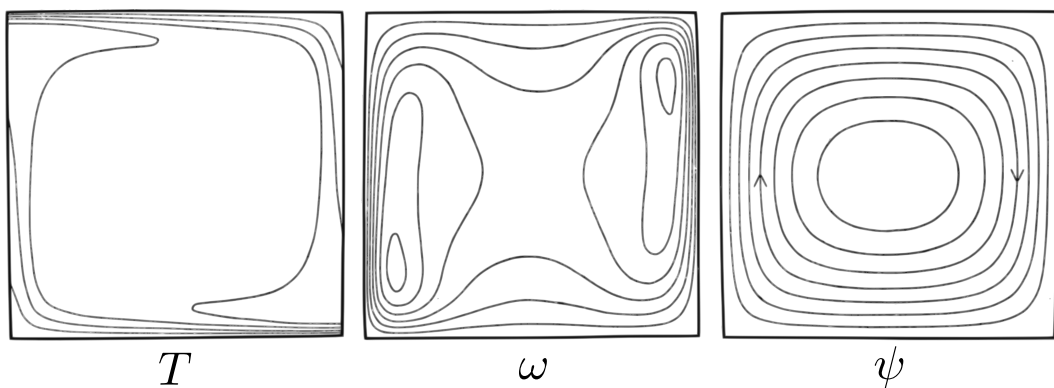


Figure 1: Numerical solution to the two-dimensional convective equations when  $\text{Ra}/\text{Ra}_c = 280$ . The three contour plots show the temperature  $T$ , the vorticity  $\omega$ , and the streamfunction  $\psi$ .

Therefore the behaviour can be approximately represented by the geometry shown in Figure 2.

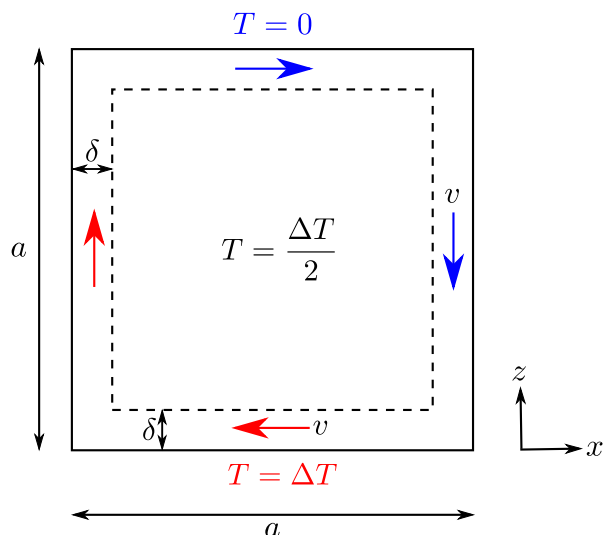


Figure 2: A schematic diagram for the scaling analysis. An isothermal, constant vorticity core region is surrounded by thin boundary layer regions of thickness  $\delta$ .

Let us recall the equations governing conservation of momentum and energy

$$0 = -\nabla \mathcal{P} + \eta \nabla^2 \mathbf{v} + \rho_0 g \alpha T \hat{\mathbf{z}}, \quad (1)$$

$$\frac{\partial T}{\partial t} + \mathbf{v} \cdot \nabla T = \kappa \nabla^2 T. \quad (2)$$

In two dimensions, we can simplify the momentum equation by taking its curl, and by introducing the vorticity  $\omega \equiv \nabla \times \mathbf{v} = (0, \omega, 0)$  to yield

$$\nabla^2 \omega = \frac{g \alpha}{\nu} \frac{\partial T}{\partial x}, \quad (3)$$

where  $\nu = \eta/\rho_0$  is the kinematic viscosity. We can simplify the energy equation by assuming that the cellular convection is steady,

$$(\mathbf{v} \cdot \nabla) T = \kappa \nabla^2 T. \quad (4)$$

The magnitude of the terms in equations (3) and (4) can be estimated from [Figure 2](#).

$$\frac{\omega}{\delta^2} \sim \frac{g \alpha \Delta T}{\nu \delta}, \quad (5)$$

$$\frac{\nu \Delta T}{a} \sim \frac{\kappa \Delta T}{\delta^2}, \quad (6)$$

where the magnitude of the vorticity is of the same order as the rotation rate of the isothermal core,

$$\omega \sim \frac{\nu}{a}. \quad (7)$$

Equations (5)-(7) give

$$\delta \sim \left( \frac{\kappa \nu}{g \alpha \Delta T} \right)^{1/3} = a \text{Ra}^{-1/3}, \quad (8)$$

$$\nu \sim a \kappa^{1/3} \left( \frac{g \alpha \Delta T}{\nu} \right)^{2/3} = \frac{\kappa}{a} \text{Ra}^{2/3}, \quad (9)$$

where

$$\text{Ra} = \frac{g \alpha \Delta T a^3}{\kappa \nu} \quad (10)$$

is the Rayleigh number. Notice that the boundary layer thickness  $\delta$  is independent of the layer thickness  $a$ .

A useful measure of the vigour of the convection is the Nusselt number Nu

$$\text{Nu} = \frac{\text{Heat transport by the convective flow}}{\text{Heat transport by conduction alone}} \quad (11)$$

The above analysis gives the ratio of the heat transports through a cell as

$$\text{Nu} \sim \frac{\rho_0 c_p \nu \Delta T \delta}{(k \Delta T/a) a} \sim \text{Ra}^{1/3}. \quad (12)$$

## Howard's boundary layer stability analysis

Convection at high Rayleigh numbers ( $\text{Ra} > 10^6$ ) is not steady, and is in fact a quasi-periodic process in which thermal boundary layers grow by thermal diffusion, become unstable, empty rapidly into plumes, at which point the cycle repeats. Thus an alternative way of obtaining a scaling between  $\text{Nu}$  and  $\text{Ra}$  is by analysing the stability of the thermal boundary layers. The boundary layer will initially grow by thermal diffusion with thickness given by

$$\delta \sim \sqrt{\kappa t}. \quad (13)$$

After a critical time  $t_c$  this boundary layer will become unstable. The criteria for this instability is that the Rayleigh number for the boundary layer exceeds the critical Rayleigh number  $\text{Ra}_c$  for convection, i.e. when

$$\text{Ra}_b \equiv \frac{g\alpha(\Delta T/2)\delta^3}{\nu\kappa} = \text{Ra}_c \approx 10^3, \quad (14)$$

the boundary layer will go unstable. This implies that the boundary layer thickness grows to

$$\delta_c \sim \left( \frac{\kappa\nu}{g\alpha\Delta T} \right)^{1/3}, \quad (15)$$

the same scaling as seen in equation (8). This occurs after a time

$$t_c \sim \kappa^{-1/3} \left( \frac{\nu}{g\alpha\Delta T} \right)^{2/3}. \quad (16)$$

The average heat flux across the boundary layer scales as

$$Q \sim \frac{k(\Delta T/2)}{\delta_c} \quad (17)$$

and hence

$$\text{Nu} \sim \frac{a}{\delta_c} = \text{Ra}^{1/3}, \quad (18)$$

just as in the previous analysis.

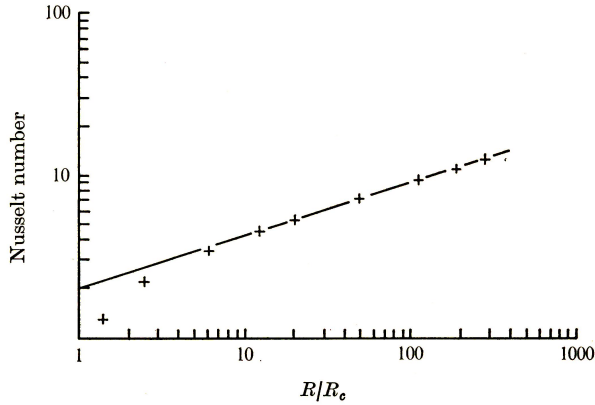


Figure 3: Results from numerical simulations, showing  $\text{Nu}$  plotted against  $\text{Ra}/\text{Ra}_c$

Figure 3 shows the results from numerical experiments, with a regression line

$$\text{Nu} = 2 \left( \frac{\text{Ra}}{\text{Ra}_c} \right)^{0.328}, \quad (19)$$

very close to the  $1/3$  scaling predicted by the simple theories. These types of  $\text{Nu}-\text{Ra}$  expressions are very useful for parameterising convective behaviour. Extensive use of such expressions has been made in calculations of the Earth's thermal history. While the simple scaling theories can predict the exponent of the  $\text{Nu} - \text{Ra}$  relationship, the prefactors must be determined by numerical or laboratory experiments.

## Thermal history calculations

The principle of convective thermal history calculations depends on the heat conservation equation

$$\frac{d}{dt} \int_V \rho c_p T dV = - \int_S Q dS. \quad (20)$$

If the Rayleigh number is large and the boundary layers thin, then, for one cell of width  $a$ , the left hand side of (20) is

$$\rho c_p a^2 \frac{d\bar{T}}{dt}, \quad (21)$$

where  $\bar{T}$  is the mean temperature of the layer. Consider what happens when the heat flux through the base of the layer is suddenly turned off. The temperature of the base of the layer then rapidly becomes the same as the interior temperature, but the structure of the boundary at the top of the layer is not affected. Therefore  $\bar{T} = \Delta T/2$ , and, by the definition of the Nusselt number, the right hand side of (20) is

$$Qa = \left( \frac{2k\bar{T}}{a} \text{Nu} \right) a = 2k\bar{T} \text{Nu}. \quad (22)$$

Boundary layer theory tells us that

$$\text{Nu} = A \text{Ra}^{1/3}, \quad (23)$$

for some numerical prefactor  $A \approx 0.2$  (Figure 3). Substituting the definition of the Rayleigh number gives

$$\text{Nu} = A \left( \frac{2g\alpha a^3}{\kappa\nu} \right)^{1/3} \bar{T}^{1/3}, \quad (24)$$

Hence (20), (21), (22) and (24) yield an ordinary differential equation describing the thermal evolution,

$$\frac{a}{2A\kappa} \left( \frac{\kappa\nu}{2g\alpha} \right)^{1/3} \frac{d\bar{T}}{dt} = -\bar{T}^{4/3}. \quad (25)$$

The time taken  $t_e$  for the layer to cool from  $T_1$  to  $T_2$  is then found by integration as

$$t_e = \frac{3a}{2A\kappa} \left( \frac{\kappa\nu}{2g\alpha} \right)^{1/3} \left( \frac{1}{T_2^{1/3}} - \frac{1}{T_1^{1/3}} \right). \quad (26)$$

## Models of mantle convection

Figures 4 and 5 show two models of mantle convection, both of which are compatible with our understanding of the fluid dynamics. Both contain cells whose aspect ratio is about one, because all laboratory and numerical experiments contain such cells. This part of the circulation is called the small scale flow. In addition the plates themselves are convective features and their motion is part of the large scale flow. If the plate motions are not decoupled from the deeper part of the mantle, the shearing that their motion produces is probably strong enough to organise the small scale flow into rolls (Figure 4). If, however, their motion is decoupled by a low viscosity zone beneath the plates, then the small scale flow should be three dimensional. These two sketches were produced before there was any way of observing the planform of the flow.

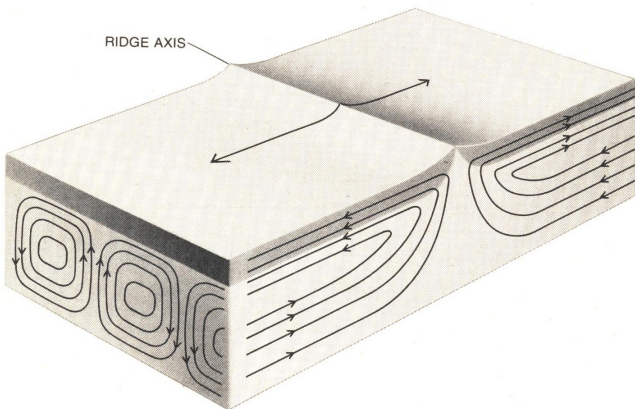


Figure 4: Possible model of convection under plates in the vicinity of a mid-ocean ridge visualises flow on two scales. If the plates are moving apart fast enough, by 10 centimetres or more a year, the small-scale convection may be transformed into longitudinal cylinders with axes parallel to the plate motion. Exactly how the large-scale convection associated with the plate motion would interact with the longitudinal convection cylinders remains to be clarified.

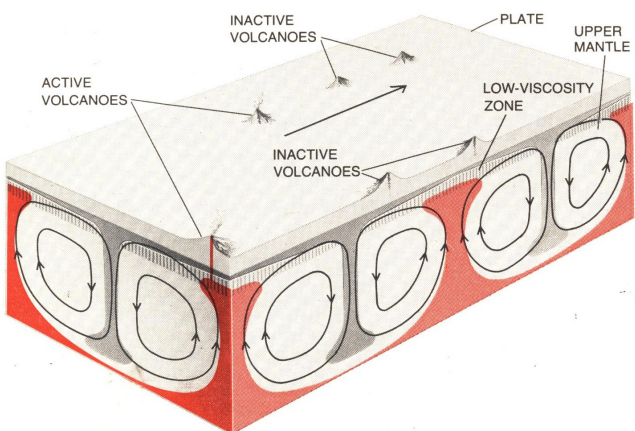


Figure 5: Alternative model of mantle convection that may explain the creation of chains of volcanoes in which the site of active volcanism does not move as fast as the plates. This diagram attempts to show only the small-scale convection cells; the large-scale circulation is omitted. The small-scale flows are somewhat decoupled from the plates by a thin, low viscosity layer that may be partially molten. Part of the heat needed to drive the small-scale circulation comes from the lower mantle and part from the decay of radioactive isotopes within the layer. Since the viscosity decreases with temperature the heat from below produces thin rising plumes of hot material. The internal heating creates cold sinking sheets and plumes, which dominate the overall flow. Because of the decoupling layer the hot rising plumes can erupt as active volcanoes that do not move with the plate, whereas lava cones of extinct volcanoes do move.

## Mapping mantle convection

The reason why the planform is hard to observe is that the flow must be ‘looked at’ through the plates. The time taken for a thermal disturbance at the base of the plate to show up as a change in heat flow at the top is about 60 Ma, by which time the plate may have moved 1000 km or more. The surface heat flux is therefore not very helpful. Nor is the plate motion itself, since plates move rigidly, even when they cover one quarter of the Earth’s surface as the Pacific does. Their motions therefore cannot reflect the details of the flow in the mantle below. Two measurements that can be made do, however, directly reflect the mantle motion beneath the plates; the gravity field and the surface elevation. The second of these reflects the flow directly, because the surface moves upwards over the rising limb of the cell, and downwards over the sinking region. The relation between the flow and the gravity field is more complicated, because the gravity is the sum of two effects.

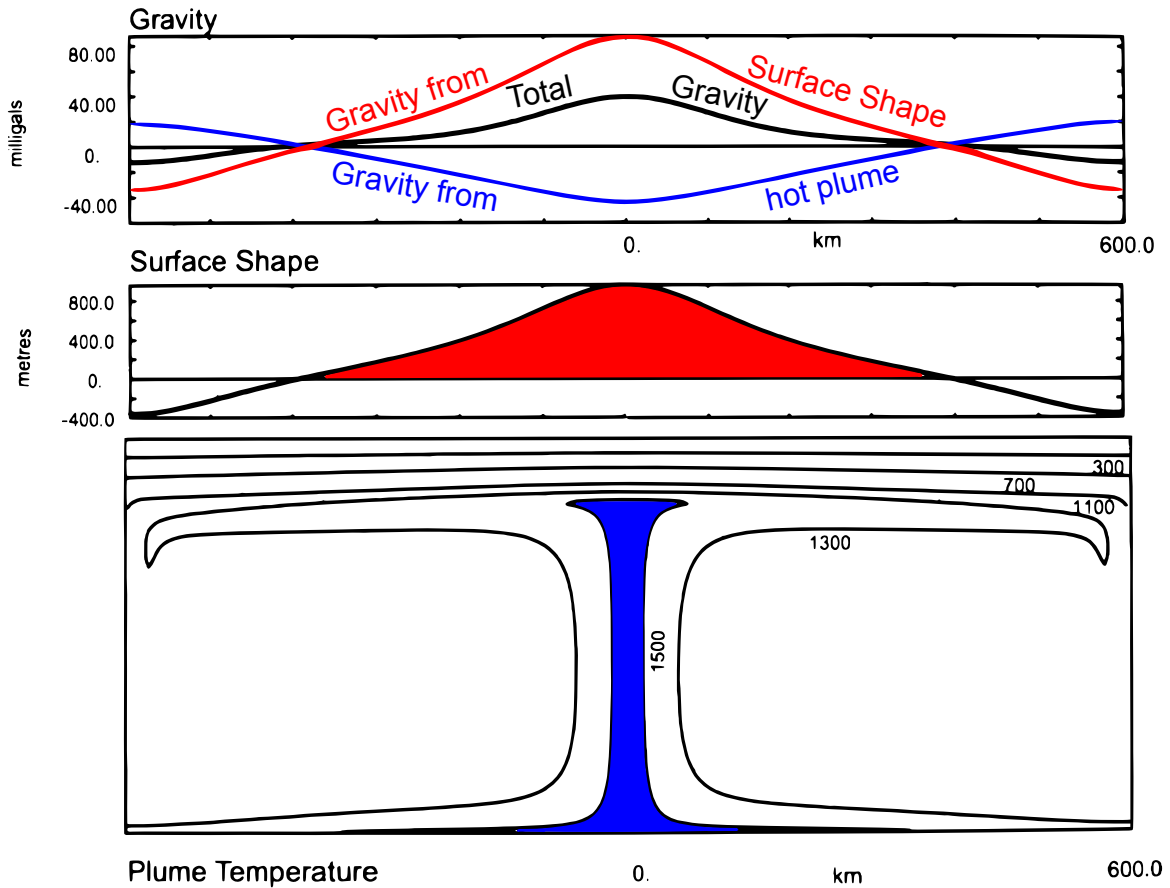


Figure 6: Fluid dynamical calculation of the temperature structure, elevation, and gravity anomaly due to a rising plume.

Figure 6 shows the gravity above a rising plume. The gravity field is produced by the temperature distribution, and is negative above the rising region. That from the surface deformation is positive above the rising region, and is somewhat larger than that due to the temperature. So the gravity is positive above the rising region, but the size of the anomaly is only about 1/3 of what would be expected from the surface deformation. This correlation between the gravity and the topography can be used to map the convective circulation. Figure 7 shows the predicted gravity and topography for a three-dimensional simulation of convection. The strong correlation between gravity and topography is clear.

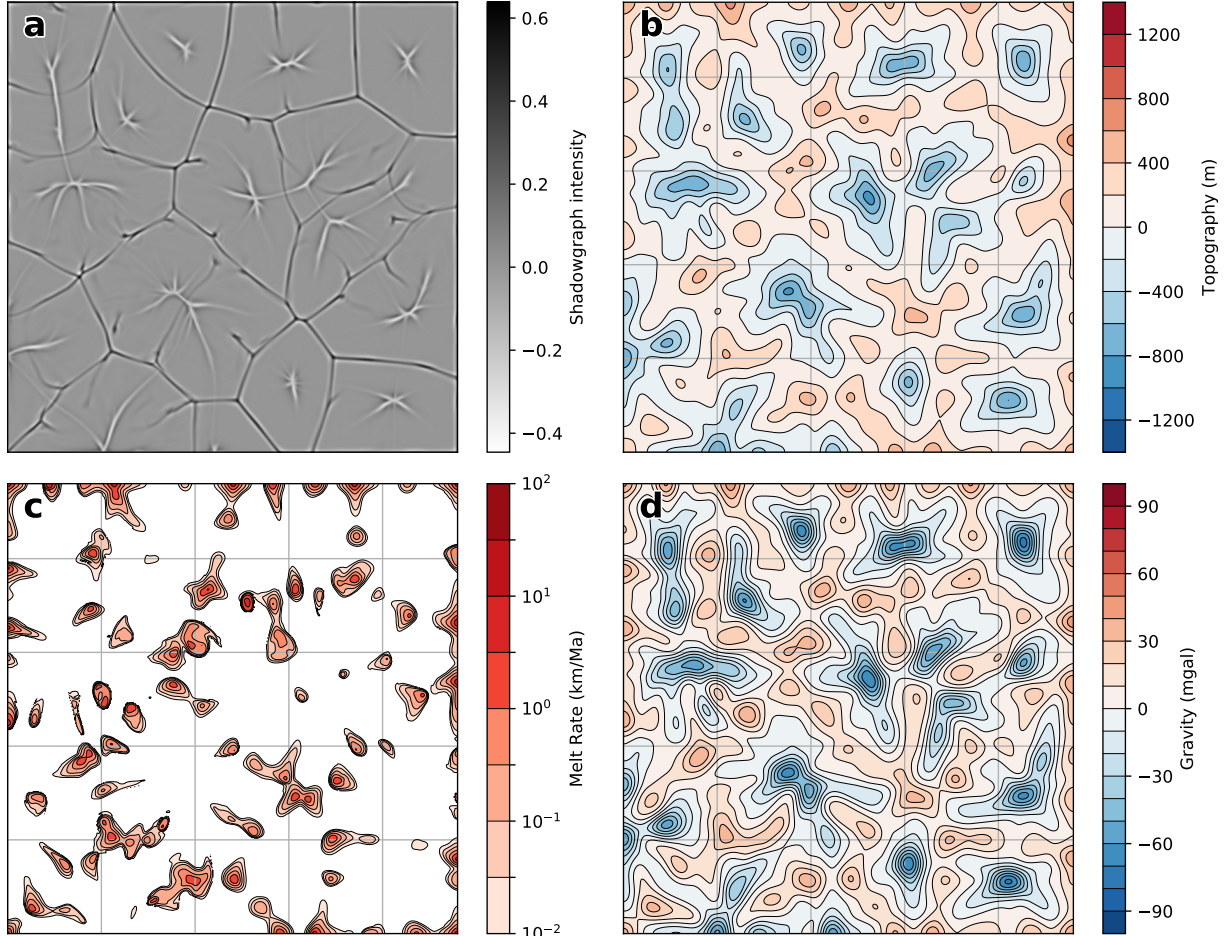


Figure 7: Maps of surface observables from a 3D numerical simulation of constant viscosity convection in a rectangular box at a Rayleigh number of  $10^6$ . The top surface of the convecting layer is freely slipping, the bottom surface is rigid. The vertical height of the box is 600 km (a value appropriate for upper mantle convection). The box is 8 times wider in the horizontal direction than in the vertical direction, so the maps above represent an area  $4,800 \text{ km} \times 4,800 \text{ km}$ . The grid lines are spaced every 1,000 km. a) shows an artificial shadowgraph, mimicking the laboratory experiments. b) shows the expected topography, and d) shows the expected gravity anomalies. Note that the surface topography and gravity are filtered by the plate on top. A lithospheric thickness of 100 km and an elastic thickness  $T_e = 30 \text{ km}$  has been assumed here. c) shows the expected pattern of melt production. Melting only occurs above the hot rising regions.

The gravity anomaly calculated from the convection models is about 30 milligals for an elevation of 1 km elevation when the topography is under water, and about 50 milligals when it is not. This correlation between gravity and topography can then be used to map the convection. The first attempts to do so were made in the North Atlantic around the Azores, using gravity and bathymetry measured by ships.

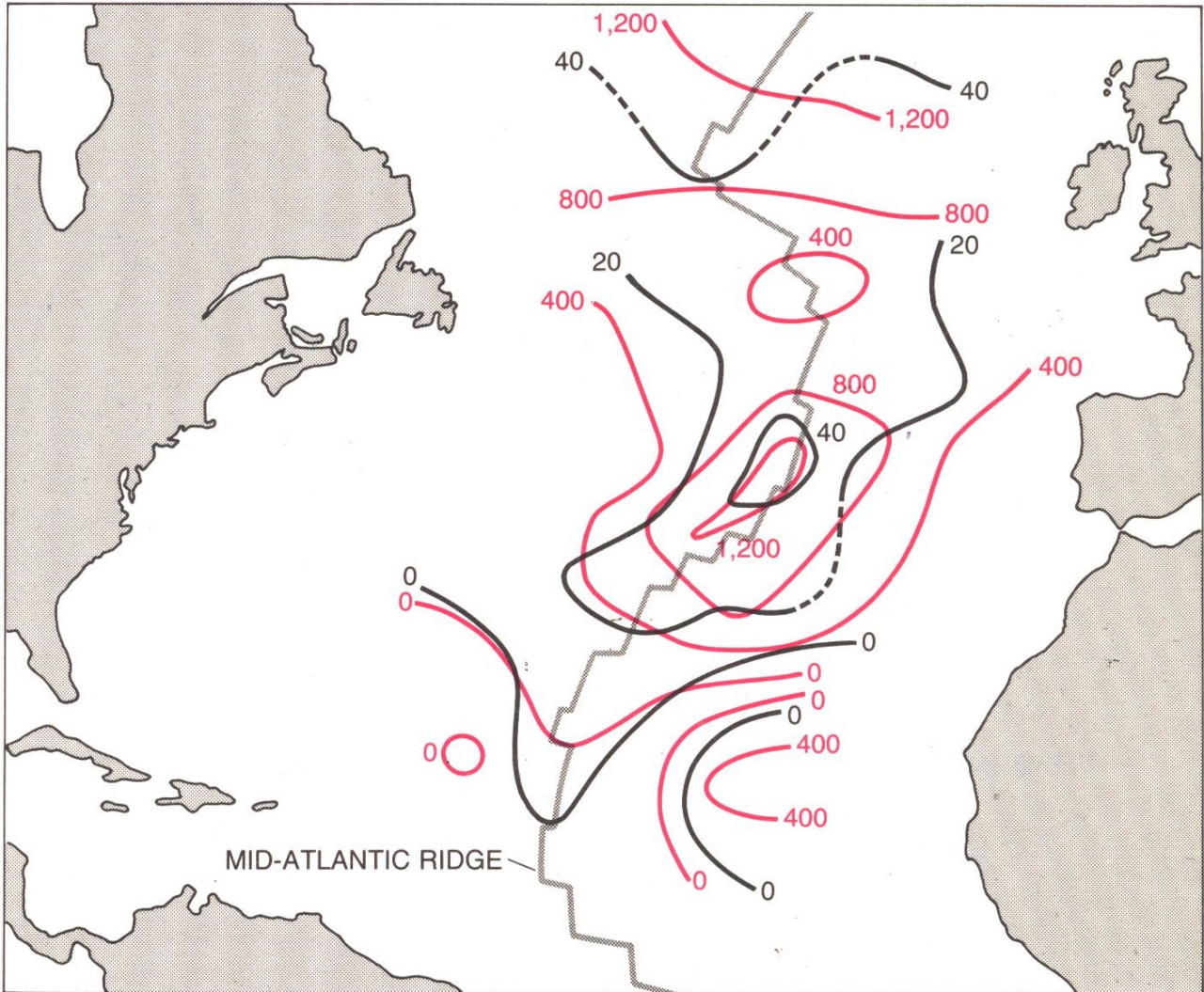


Figure 8: Depth of the North Atlantic is shown in metres (red) after removal of the effect of cooling of the plate by age. Black lines show contours of the gravity field in milligals. The variations in the two features seem to be closely related and could be evidence for a region in which hot mantle material is carried upward by small-scale convection currents. Neither the depth of the ocean nor the gravity field seems to bear much relation to the Mid-Atlantic Ridge (grey line), where the North American plate and the Eurasian plate are being pushed apart.

The contour plot Figure 8 shows the free air gravity averaged over regions of about 500 km  $\times$  500 km in black, with the values on the contours in milligals, together with the bathymetry, corrected for plate contraction as a function of age. When the depths have been corrected in this way they are known as *residual depths*. The correlation between gravity and topography is clear, and relationship between the two is approximately the same as that calculated for the convective models. The convective gravity anomalies are easily distinguished from the larger, but shorter wavelength, anomalies due to flexure (Figure 9).

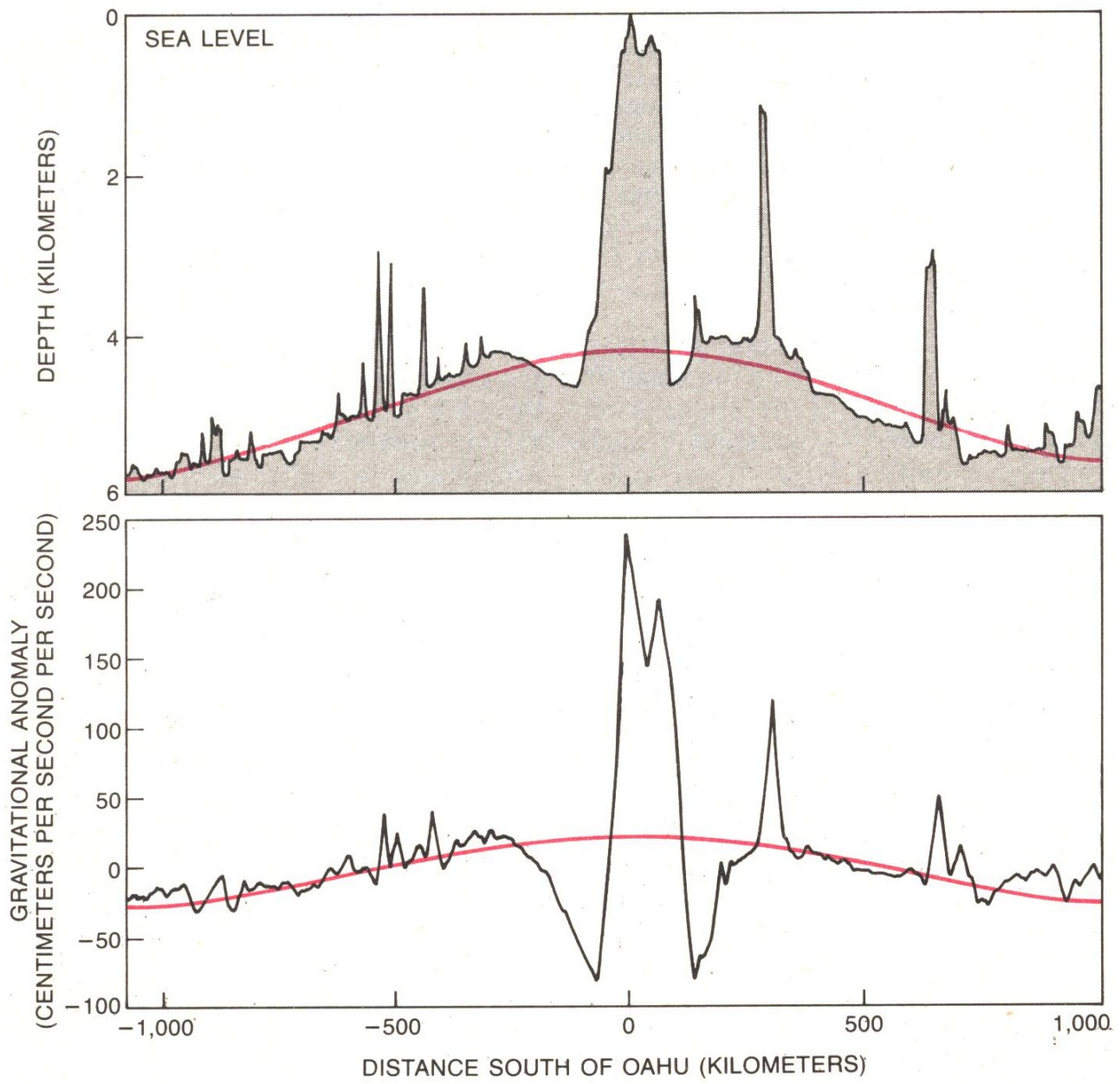


Figure 9: The elastic response of a plate to stresses that are unrelated to convection in the mantle must be understood before the effects of upwelling or downwelling in the mantle can be observed. For example, the weight of the Hawaiian ridge causes a depression of the sea floor on both flanks of the ridge, which can be seen in the profiles of both the bathymetry and the gravitational anomaly north and south of the island of Oahu. The deflection caused by the ridge is confined to within about 200 km of the load. Hence it can be inferred that the rigidity of the plate is not great enough for local loads to generate variations in depth or gravity at greater distances. Both profiles also show that the Hawaiian ridge and the neighbouring depressions are superposed on a broad swell, which is generally thought to be the surface expression of a hot, upwelling region in the mantle. The swell can be best observed if fluctuations in the bathymetry and gravitational anomaly shorter than 500 km are smoothed (red curves).

As so often happens in geophysics, a new instrument became available that solved the problem of the measurement of gravity at sea. It was an altimeter that was carried on a satellite, and could map the gravity field directly by mapping the shape of the sea surface, which to a good approximation is an equipotential. The instrument works by measuring the time it takes for a radar pulse to travel from the dish of the satellite to the sea surface and back. The area of the sea from which the reflection is returned (or *footprint*) is a few kilometres across, and the distance can be measured to a precision of about 10 mm if the waves are not too high. The shape of the sea surface can only be determined if the location of the satellite is known, and the accuracy of the measurement is still limited by this problem. Navigation has improved steadily, and the average error in height is now about 10 mm.

[Figure 10](#) shows one of the first such satellites, GEOS 3. The ring of small white circles round the satellite are optical corner cubes, so that it can be tracked by laser ranging, and the Y shaped aerials emit a constant frequency radio wave so that it can also be tracked by Doppler. The single aerial surrounded by the four helical wires is for transmitting the data to the ground.



Figure 10: Two satellites used for measuring the gravity field of the Earth. On the left is GEOS 3, a NASA satellite launched in 1975. On the right is GOCE, an ESA satellite, that was in orbit from 2009-2013.

[Figure 10](#) also shows GOCE, the most recent ESA gravity satellite. GOCE measured the Earth's gravity field over both land and sea using a combination of an on-board gravity gradiometer and GPS tracking.

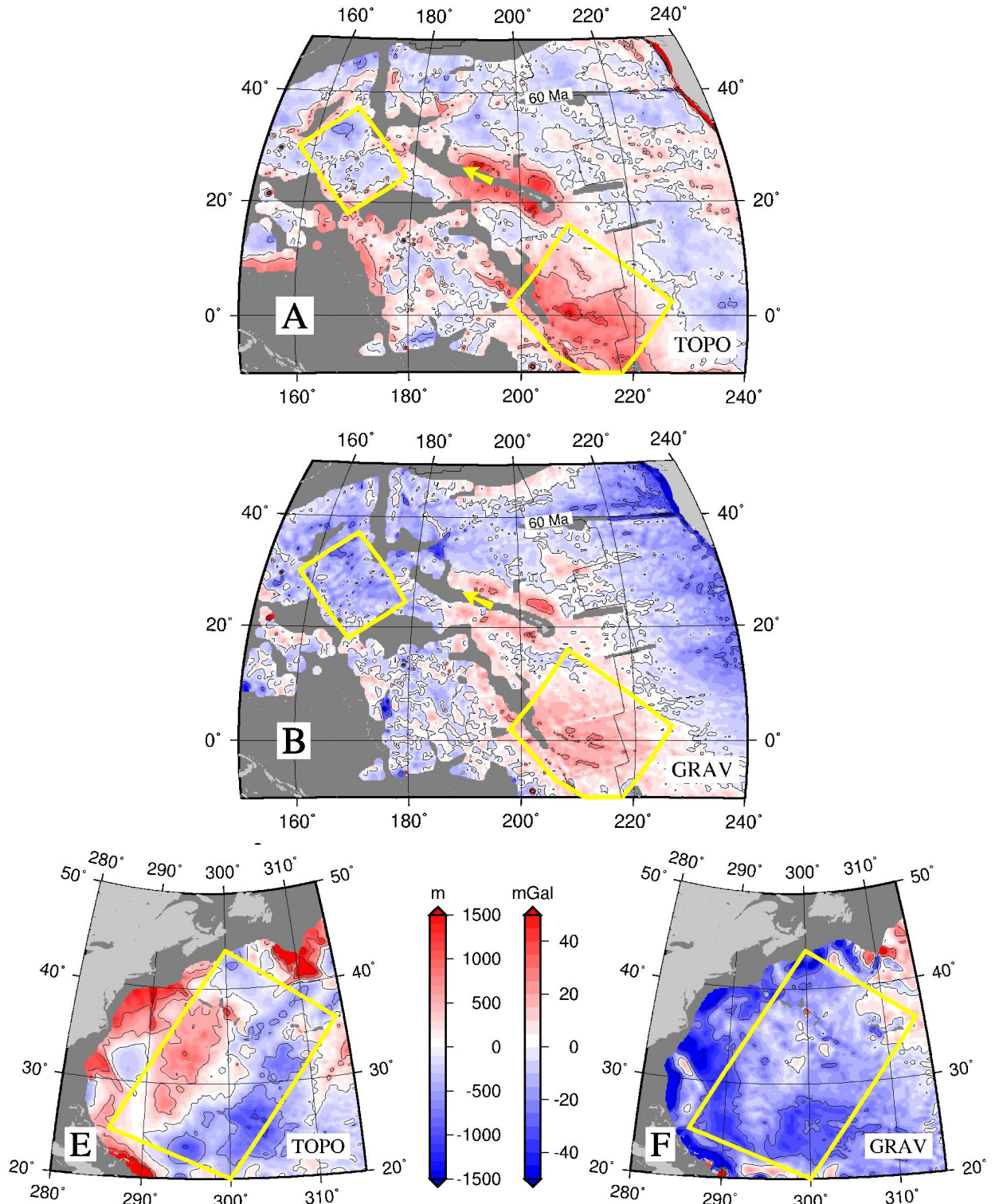


Figure 11: Maps of the Pacific (A and B) and the western North Atlantic (E and F) produced from the satellite measurements of the gravity field and residual depths from ship tracks clearly show patterns of positive and negative gravity and residual depth anomalies resulting from mantle convection. The wavelength of such anomalies is typically 2000–3000 km, and therefore have an aspect ratio of 1.5–2 if the convection is restricted to the upper mantle. The maps clearly show that the convective circulation mapped by the gravity and topography has a smaller scale than that of the plate motions.

The two maps in Figure 11A and B show residual depth and gravity anomalies for the Pacific. If the planform were rolls, you would see linear anomalies running across the map in the direction of the plate motion (yellow arrow). The anomalies are only slightly elongated in the direction of motion, and the planform must therefore be three dimensional. The Pacific plate covers most of the map, so it is clear that there must be a small scale flow whose scale is much smaller than that of the Pacific.

In most continental regions the topography is principally controlled by variations in crustal thickness, rather than by mantle convection. But gravity anomalies with wavelengths of more than about 500 km cannot be supported by elastic stresses in the lithosphere, and so can be used to map the convective circulation directly. Figure 12 shows such a map for the African plate, and clearly shows that the convective circulation is not related to the geometry of the ridges, which surround Africa.

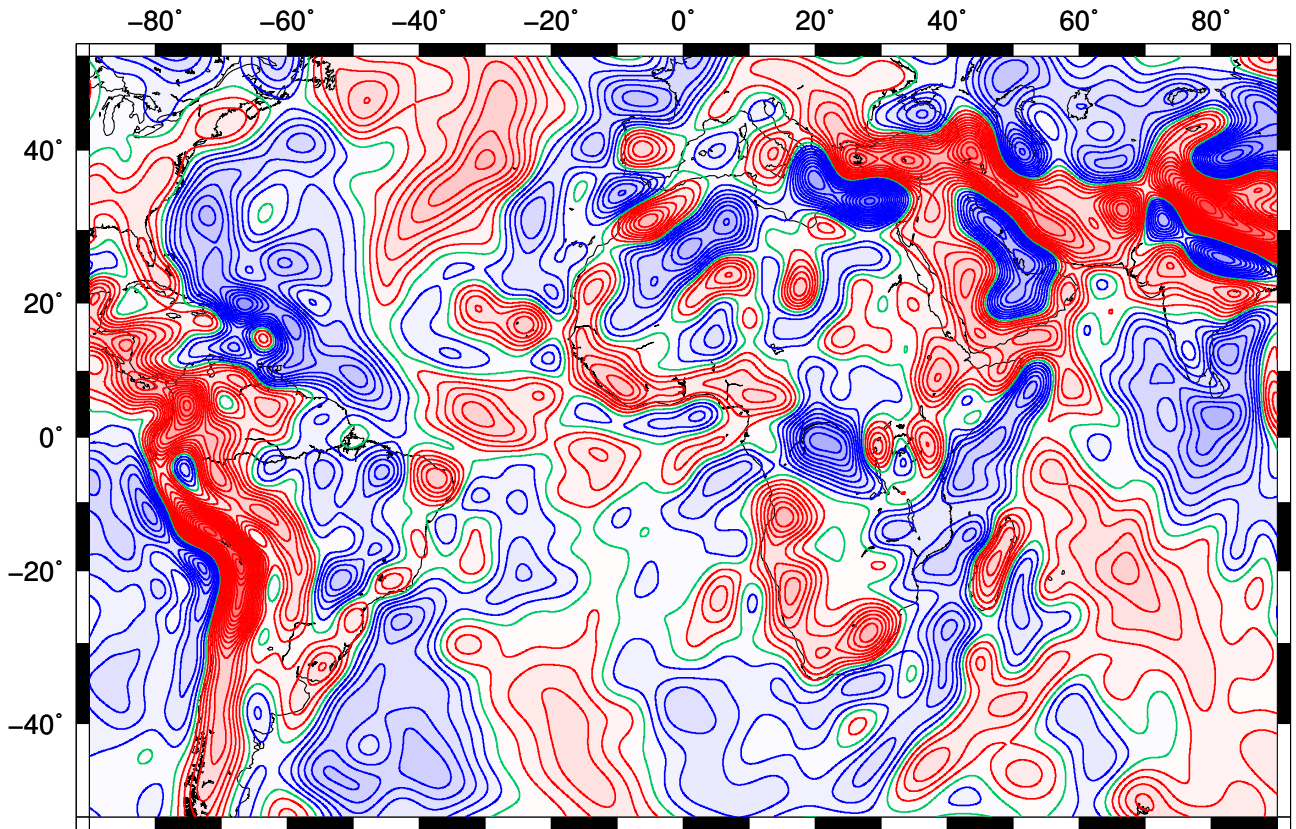


Figure 12: Long wavelength ( $>800$  km) free air gravity anomaly map of the African plate. Red, green, and blue shaded contours represent positive, zero, and negative gravity anomalies. Contour interval is 5 mGal.

The small linear positive gravity anomalies along the ridges are produced by the density variations associated with the spreading ridges themselves, even though the ridges are isostatically compensated, and are not the result of thermal upwelling in the upper mantle. The picture shows that there are many rising and sinking plumes beneath Africa. Because Africa has been tectonically stable for a long time and all the tectonic topography has been removed by erosion, the convective circulation is reflected in the topography.

## Depth-Age Revisited

Small scale convective flow has been used to explain the variation of depth with age (Figure 13). The depth of the sea floor is less than would be expected from the cooling half space model when the age of the plate is greater than about 80 Ma. The observations agree well with the predicted behaviour of a cooling plate, where the temperature at a depth of about 100 km remains constant. One way in which the base of the plate can be kept warm is by small scale convective transport. Such convection can be driven by boundary layer instabilities as the plate thickens with age (Figures 14 and 15).

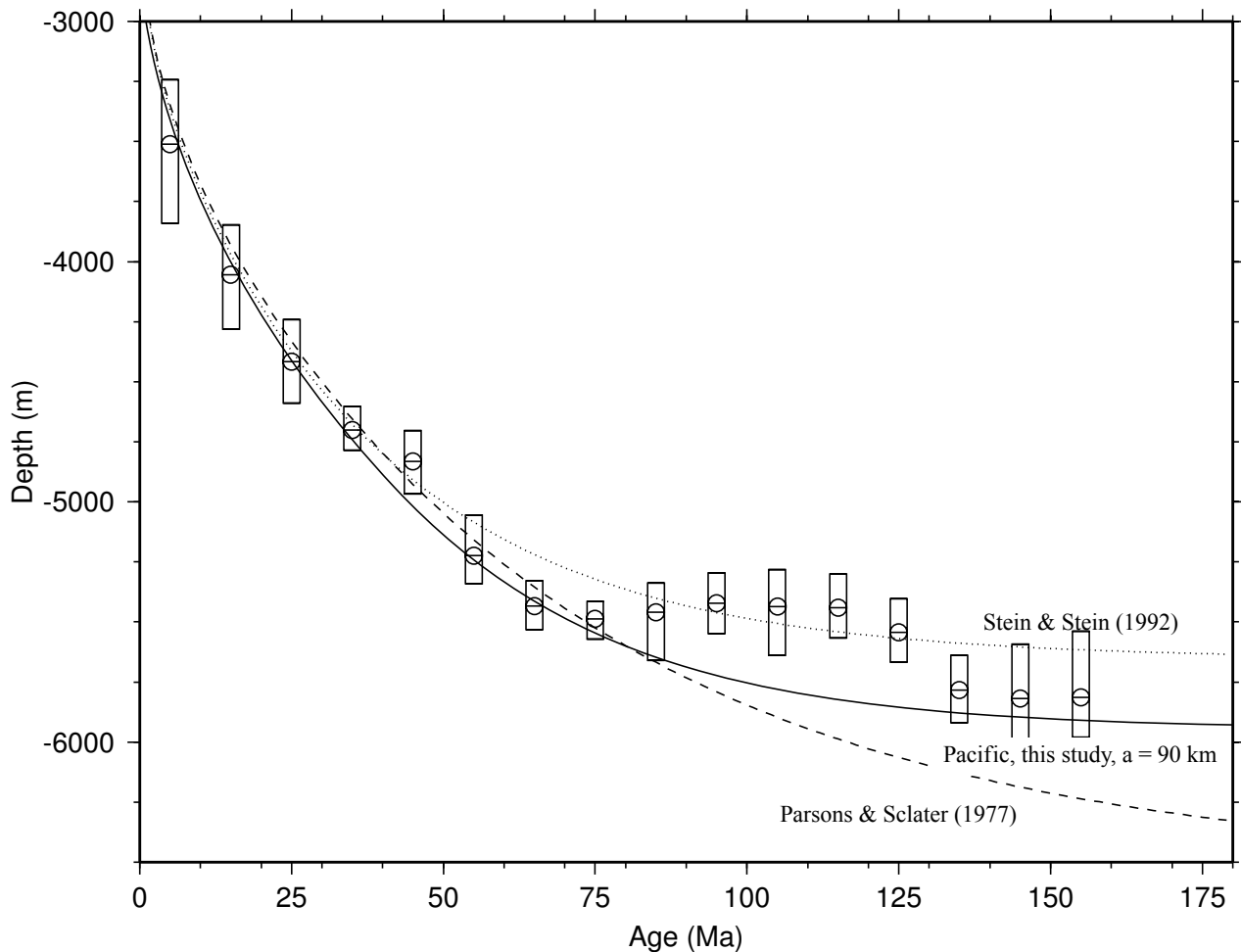


Figure 13: A recent compilation of depth versus age data for the Pacific plate (circles with error bars). Lines show a series of plate model curves proposed by different authors. The solid line is the fit preferred by Crosby et al. (2006), which has a plate thickness of 90 km. Notice the flattening with age, and also the “overshoot” between 80 and 130 Ma.

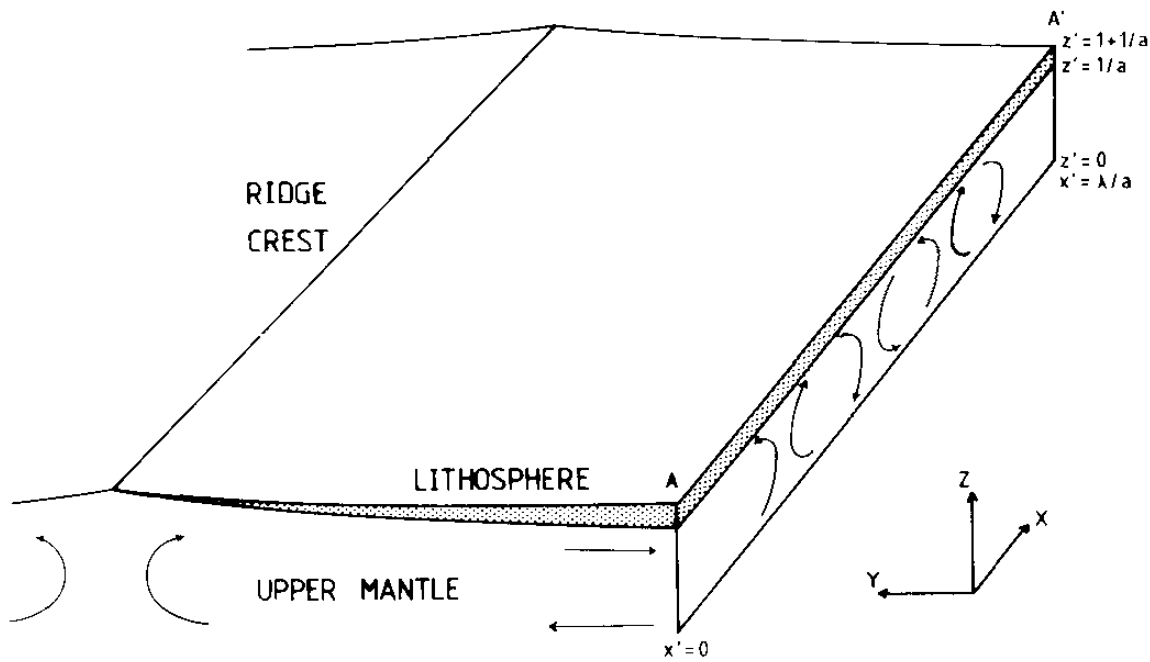


Figure 14: Sketch of two-scale convection in the upper mantle underlying oceanic lithosphere. The arrows show the sense of motion of a possible flow field restricted to the upper mantle. As the upper thermal boundary layer grows it becomes unstable and small scale convection develops.

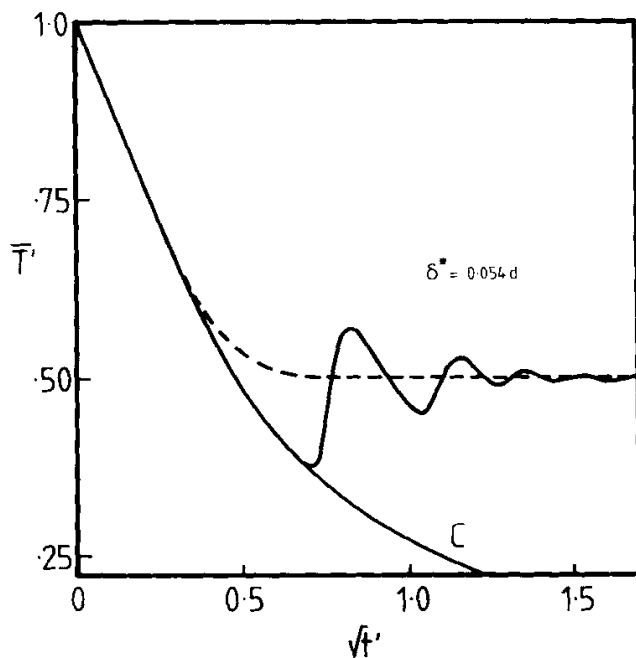


Figure 15: The subsidence history of the model depicted in Figure 14, shown by the unmarked continuous line, agrees with the subsidence history of the plate model, shown dashed, and is quite different from that of the cooling half space model, marked C. There is also a hint that the “overshoot” seen in Figure 13 may be explained by this convective model.